Quantum Annealing and Thermalization: Insights from Integrability

Fuxiang Li, Vladimir Y. Chernyak, and Nikolai A. Sinitsyn

Phys. Rev. Lett. **121**, 190601 — Published 6 November 2018

DOI: 10.1103/PhysRevLett.121.190601

Quantum annealing and thermalization: insights from integrability

Fuxiang Li
School of Physics and Electronics, Hunan University, Changsha 410082, China
Theoretical Division, Los Alamos National Laboratory, B213, Los Alamos, NM 87545 and
Center for Nonlinear Studies, Los Alamos National Laboratory, Los Alamos, NM 87545

Vladimir Y. Chernyak
Department of Chemistry and Department of Mathematics,
Wayne State University, 5101 Cass Ave, Detroit, Michigan 48202, USA

Nikolai A. Sinitsyn
Theoretical Division, Los Alamos National Laboratory, B213, Los Alamos, NM 87545
(Dated: October 12, 2018)

We solve a model that has basic features that are desired for quantum annealing computations: entanglement in the ground state, controllable annealing speed, ground state energy separated by a gap during the whole evolution, and programmable computational problem that is encoded by parameters of the Ising part of the spin Hamiltonian. Our solution enables exact nonperturbative characterization of final nonadiabatic excitations, including scaling of their number with the annealing rate and the system size. We prove that quantum correlations can accelerate computations and, at the end of the annealing protocol, lead to the perfect Gibbs distribution of all microstates.

Many optimization problems can be reformulated in terms of searching for a configuration that minimizes a Hamiltonian $H_A(s_1,\dots,s_N)$ of N Ising spins s_j [1–3]. This task is often so complex that it cannot be solved with modern computers. The idea of quantum annealing (QA) is to treat the Ising spins as z-components of quantum spins-1/2, $\hat{\boldsymbol{s}}_j$, and realize quantum evolution with a Hamiltonian

$$\hat{H}(t)=\hat{H}_A(\hat{s}_1^z,\dots,\hat{s}_N^z)+g(t)\hat{H}_B(\hat{\boldsymbol{s}}_1,\dots,\hat{\boldsymbol{s}}_N), \quad (1)$$

where $\hat{H}_B$ has a ground state that overlaps with all possible QA outcomes and does not discriminate against some of them at the start. Parameter $g(t)$ is large at $t=0$ but decays to zero at $t\to\infty$. According to the adiabatic theorem, a system that is initially in the ground state remains in the instantaneous ground state if the lowest energy is always nondegenerate and parameters change sufficiently slowly. So, as we illustrate in Fig. 1(a), slow decay of $g(t)$ converts the ground state of $\hat{H}_B$ into the ground state of $\hat{H}_A$, which is then read by measuring spins along the z-axis.

In practice, the annealing time is restricted, so nonadiabatic excitations become inevitable [4–7]. Nevertheless, at $N\gg 1$, there are optimization problems with some error tolerance. In this letter, we solve a minimal model of QA and show that:

(i) tolerance of a computational goal to a small number of errors allows QA protocols that introduce extra quantum correlations in order to reduce the required computation time by a factor $\sim 1/N$ in comparison to the conventionally justified QA time.

(ii) the distribution of nonadiabatic excitations in a closed quantum system after QA can be completely thermalized;

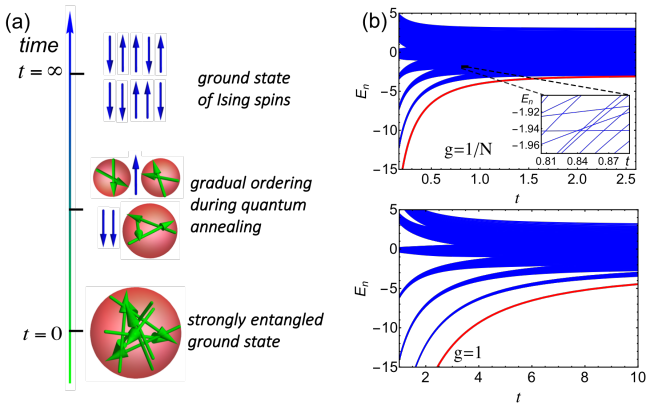

FIG. 1. **(a)** During QA, the entangled ground state is transformed adiabatically into the ground state of the Ising spin Hamiltonian. **(b)** Evolution of the spectra of the QA Hamiltonian (3) in nonadiabatic ($g=1/N$, top) and nearly-adiabatic ($g=1$, bottom) regimes. The ground level is marked by red color. Here, $N=12$, $S^z_{\rm tot}=0$, $\varepsilon_j=j/N+\xi_j$, and ξ_j are uniformly distributed random real numbers from the range $(-1/(2N),1/(2N))$. The inset shows exact level crossings indicating model's integrability.

(iii) this thermalization is encoded in integrability, i.e., the possibility to describe the behavior analytically.

The first property justifies the error-tolerant QA computation technology, the second one proves that averaging over unknown conditions is not needed to find thermalization in coherent evolution, and the third one counters the common belief, taking roots in the numerical experiment by Fermi-Pasta-Ulam-Tsingou [8], that complete thermalization is incompatible with integrability.

Initial quantum correlations are not required for QA but our goal here is to learn if they can be a resource

for accelerated computations. The simplest Hamiltonian of N spins with entanglement in the ground state is all-to-all coupling [9–11], $\hat{H}_B = -\sum_{i\neq j}^{N} \hat{s}_i^+ \hat{s}_j^-$, restricted to a sector with a conserved total spin. The ground state of $\hat{H}_B$ is the sum of all eigenstates of $\hat{H}_A$ with the same $S^z_{\rm tot} = \sum_{j=1}^{N} s_j^z$:

$$|\psi_0\rangle \sim |\uparrow\uparrow\ldots\downarrow\downarrow\rangle + |\uparrow\downarrow\ldots\uparrow\downarrow\rangle + \ldots + |\downarrow\downarrow\ldots\uparrow\uparrow\rangle. \quad (2)$$

The simplest to write QA protocol is the inverse time decay, $g(t) = g/t$, where $t \in (0_+, \infty)$, g is a constant; and the simplest Ising Hamiltonian is $\hat{H}_A = \sum_{j=1}^{N} \varepsilon_j \hat{s}_j^z$, where the vector of constant parameters, $\boldsymbol{\varepsilon} = (\varepsilon_1, \ldots, \varepsilon_N)$, is programmable for computations. So, the minimal QA Hamiltonian for our goals is

$$\hat{H}_{\rm BCS}(t) = \sum_j \varepsilon_j \hat{s}_j^z - \frac{g}{t} \sum_{j\neq k} \hat{s}_j^+ \hat{s}_k^-, \quad j,k = 1,\ldots,N. \quad (3)$$

Let $S^z_{\rm tot} = 0$ and all constants ε_j be nondegenerate. The ground state of H_A has then $N/2$ spins down and $N/2$ spins up; all down-spins have larger ε_j than all up-spins. Hence, QA with $\hat{H}_{\rm BCS}$ solves an array sorting problem: to find $N/2$ indices j that mark the largest ε_j.

The time-*in*dependent version of $\hat{H}_{\rm BCS}$ is equivalent to the Bardeen-Cooper-Schrieffer model of superconductivity [12]. Its nonequilibrium dynamics has attracted considerable interest both experimentally [13, 14] and theoretically [15, 16]. Recently, the time-dependent model (3) was proved to be integrable [17], but its solution for arbitrary t in terms of repeated contour integrals [18] is too complex to reveal physical properties of QA. Therefore, here we will develop a different approach that will target the desired characteristics directly.

Deviation from adiabaticity is controlled continuously in $\hat{H}_{\rm BCS}(t)$, as shown in Fig. 1(b): the ground level is always separated by a gap from the rest of the spectrum but approaches other levels slower when g is larger. Precision of QA is usually characterized by the probability P_G to remain in the ground state at $t \to \infty$. According to the Landau-Zener formula, P_G is determined by the size of the energy distance Δ to the nearest energy level and the characteristic rate β with which this gap changes: $P_{LZ} = 1 - e^{-2\pi\Delta^2/\beta}$. At $t \to \infty$, the ground level of $\hat{H}_{\rm BCS}$ is separated from the lowest energy excitation by $\Delta = |\varepsilon_i - \epsilon_j|$, where i and j are indexes of spins for which this energy difference is minimal. Coupling between these spins becomes comparable to Δ at the effective annealing time $\tau \sim g/\Delta$, and the characteristic rate with which this coupling changes is $\beta = |d(g/t)/dt|_{t=\tau} = \Delta^2/g$. This leads to the rough estimate in the adiabatic limit: $P_G \sim 1 - e^{-2\pi g}$, which we confirm in Fig. 2(a) by comparing to numerical results. Hence, values $g > 1$ correspond to adiabatic QA.

To understand the regime at $g < 1$, we assume in what follows that $0 < \varepsilon_1 < \varepsilon_2 < \ldots < \varepsilon_N$, and introduce a new

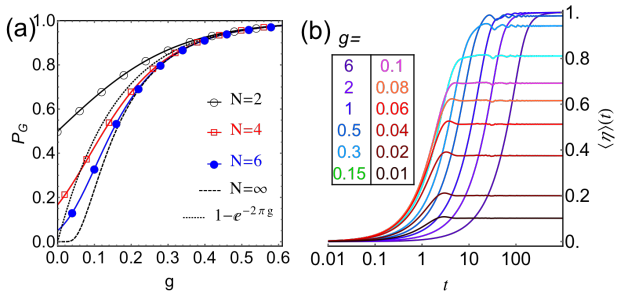

FIG. 2. **(a)** The probabilities to remain in the ground state at different g and N. Solid curves and the limit $N \to \infty$ (black dashed curve) are predictions of Eq. (12) and point markers are the numerical results [19]. **(b)** Time-dependence of computation accuracy. Solid curves are results of the numerical solution for the Hamiltonian $\hat{H}_{\rm BCS}(t)$ with $N = 12$, $S^z_{\rm tot} = 0$, and the same ε_j as in Fig. 1(b).

accuracy characteristic:

$$\eta \equiv (4/N) \sum_{k=1}^{N/2} s_k^z, \quad (4)$$

where s_k^z is the outcome of the k-th spin polarization measurement. The ground state of $\hat{H}_A$ at $S^z_{\rm tot} = 0$ has $\eta = 1$. Excitations reduce η, e.g., $\eta = 0$ means complete loss of valuable information.

In Fig. 2(b) we show time-dependence of the mean value $\langle\eta\rangle$ at different g, obtained by solving the Schrödinger equation with $\hat{H}_{\rm BCS}$ for $N = 12$ numerically. Saturation of $\langle\eta\rangle$ means that one can interrupt evolution at finite t without loosing accuracy. Final $\langle\eta\rangle$ is growing with g and at $g = 1/N$ it reaches values $\langle\eta\rangle > 0.6$, at which over 80% of spins point correctly along their ground state directions. At $g < 1/N$, the time to saturation is mostly defined by the energy parameters ε_j and almost does not change with g. For $g > 1/N$, this time is growing and becomes about a factor N longer at $g = 1$ than at $g = 1/N$, in agreement with our rough estimate $\tau \sim g/\Delta$. Figure 2(b) also suggests that $\langle\eta\rangle = 1 - O(1/N)$ is reached at values of g outside the adiabatic regime. However, numerical simulations are not decisive here because they are restricted to small N. So, we will develop an analytical approach that will confirm this expectation.

To understand behavior at arbitrary N, we recall that $\hat{H}_{\rm BCS}$ commutes with N Gaudin Hamiltonians [20]:

$$\hat{H}_j = t\hat{s}_j^z - 2g \sum_{k\neq j} \frac{\hat{\mathbf{s}}_j \cdot \hat{\mathbf{s}}_k}{\varepsilon_j - \varepsilon_k}, \quad k,j = 1,\ldots,N,$$

which also satisfy conditions: $\partial_{\varepsilon_j} \hat{H}_{\rm BCS} = \partial_t \hat{H}_j$ and $\partial_{\varepsilon_j} \hat{H}_i = \partial_{\varepsilon_i} \hat{H}_j$ for all i,j. According to [17], this property is what makes the model (3) analytically solvable. Following [17], we introduce multi-time vector $\boldsymbol{t}$, where

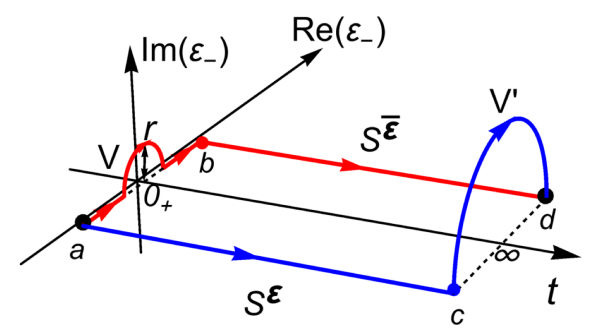

FIG. 3. Two paths corresponding to the same evolution operator. Evolution takes place over the space of real time t and complex values of $\varepsilon_- \equiv \varepsilon_j - \varepsilon_{j+1}$. The initial point a corresponds to $t = 0_+$ and $\varepsilon_j < \varepsilon_{j+1}$. The final point d is at $t \to \infty$ and $\bar{\varepsilon}_j = \varepsilon_{j+1}$, $\bar{\varepsilon}_{j+1} = \varepsilon_j$. The red path $a \to b \to d$ avoids the singularity at $\varepsilon_- = 0$ from the infinitesimally small distance r at $t = 0_+$, and the blue path $a \to c \to d$ avoids this singularity at $t \to \infty$ along the arc (cd) with a finite radius. Evolution over links (ab), (bd), (ac), and (cd) is described by matrices, respectively, V, $S^{\bar{\boldsymbol{\varepsilon}}}$, $S^{\boldsymbol{\varepsilon}}$, and V'.

$t^0 \equiv t$, $t^j \equiv \varepsilon_j$ and write an operator of evolution in this multi-time space

$$\hat{U} = \hat{\mathcal{T}} \exp\left[-i \int_{\mathcal{P}} \sum_{\mu=0}^{N} \hat{H}_\mu \, dt^\mu\right], \quad \hat{H}_0 \equiv \hat{H}_{\rm BCS}.$$

$\hat{U}$ does not depend on the path $\mathcal{P}$, except its initial and final points. This invariance follows from the fact that the gauge field with components $\mathcal{A}_\mu = -i\hat{H}_\mu$ has zero curvature. Hence, its integral over any closed path that does not enclose singularities of $\hat{H}_\mu$ is zero [17].

Let us compare two evolution paths shown in Fig. 3 that start at vector $\boldsymbol{\varepsilon}$ at $t = 0_+$ (point a) and end at $t \to \infty$ at vector $\bar{\boldsymbol{\varepsilon}}$ (point d) such that two adjacent in magnitude vector components are related by $\bar{\varepsilon}_j = \varepsilon_{j+1}$ and $\bar{\varepsilon}_{j+1} = \varepsilon_j$ for one and only one j, while in all other respects $\boldsymbol{\varepsilon}$ and $\bar{\boldsymbol{\varepsilon}}$ are identical. These paths have to avoid the singularity of $\hat{H}_j - \hat{H}_{j+1}$ at $\varepsilon_j = \varepsilon_{j+1}$, so the difference $\varepsilon_- \equiv \varepsilon_j - \varepsilon_{j+1}$ is allowed to be complex valued.

At the path $a \to b \to c$, evolution matrix V along the link (ab) reverses the sign of ε_- keeping other parameters constant. Next, at (bc), we keep $\bar{\boldsymbol{\varepsilon}}$ constant and evolve to the end point at $t \to \infty$ with the evolution matrix $S^{\bar{\boldsymbol{\varepsilon}}}$. At the other path $a \to c \to d$ we initially evolve, with the evolution matrix $S^{\boldsymbol{\varepsilon}}$, along the real time to a point at large t and then reach the end point, with the evolution matrix V', at constant t. The invariance of $\hat{U}$ means that

$$S^{\bar{\boldsymbol{\varepsilon}}} V |\psi_0\rangle = V' S^{\boldsymbol{\varepsilon}} |\psi_0\rangle. \tag{5}$$

We will use Eq. (5) to compare amplitudes of evolution along real t from $|\psi_0\rangle$ to states $|j\rangle = |\ldots, \uparrow_j, \downarrow_{j+1}, \ldots\rangle$ and $|\tilde{j}\rangle = |\ldots, \downarrow_j, \uparrow_{j+1}, \ldots\rangle$ that are different only by directions of two spins with neighboring ε_j and ε_{j+1}.

Consider first the link (ab) in Fig. 3. Suppose that initially $\varepsilon_j < \varepsilon_{j+1}$. We keep $\varepsilon_j + \varepsilon_{j+1}$ constant, so

$$\int \hat{H}_j \, d\varepsilon_j + \int \hat{H}_{j+1} \, d\varepsilon_{j+1} = (1/2) \int (\hat{H}_j - \hat{H}_{j+1}) \, d\varepsilon_-.$$

The evolution operator for this link is

$$V = \hat{\mathcal{T}} \exp\left[-(i/2) \int_{\mathcal{P}_{(ab)}} (\hat{H}_j - \hat{H}_{j+1}) \, d\varepsilon_-\right]. \tag{6}$$

All $\hat{H}_\mu$ commute, so $|\psi_0\rangle$ is the eigenstate of not only $\hat{H}_{\rm BCS}$ but also of $\hat{H}_j - \hat{H}_{j+1}$. Hence, $\langle\alpha|(\hat{H}_j - \hat{H}_{j+1})|\psi_0\rangle = 0$ for $|\alpha\rangle \perp |\psi_0\rangle$. We calculate $|\langle\psi_0|V|\psi_0\rangle|$ bypassing the singularity at $\varepsilon_j = \varepsilon_{j+1}$ along the semicircle of radius r in the complex ε_- plane. Only the piece of this path with nonzero $\mathrm{Im}(\varepsilon_-)$ contributes to the absolute value. In the limit $r \to 0$ at $t = 0$, we have $\hat{H}_j - \hat{H}_{j+1} \to -4g\hat{\boldsymbol{s}}_j \cdot \hat{\boldsymbol{s}}_{j+1}/\varepsilon_-$. For $\varepsilon_- = re^{i\phi}$, we find

$$|\langle\psi_0|V|\psi_0\rangle| = e^{(1/2)\int_\pi^0 d\phi \, \langle\psi_0|(\hat{H}_j - \hat{H}_{j+1})|\psi_0\rangle_{t=0}} = e^{\pi g/2}. \tag{7}$$

Consider now the link (cd), at which $t \to \infty$. If $n \neq j, j+1$ we have $\hat{H}_n = ts_n^z + O(1)$. Hence, such Hamiltonians are proportional to spin operators, and commutation of $\hat{H}_n$ with $\hat{H}_j - \hat{H}_{j+1}$ means conservation of s_n^z during the evolution along this link, i.e., $\langle j|V'|\alpha\rangle = 0$ if $|\alpha\rangle$ has different from $|j\rangle$ value of a spin with index n. Transitions between states $|j\rangle$ and $|\tilde{j}\rangle$, however, should be treated with extra care because $\hat{H}_j$ and $\hat{H}_{j+1}$ are singular near $\varepsilon_j = \varepsilon_{j+1}$ where conservation of spins with indexes j and $j+1$ breaks down. So, we set evolution between points c and d along a semicircle with a finite radius in Fig. 3, restricting this evolution to the subspace of states $|j\rangle$ and $|\tilde{j}\rangle$.

Let us again change variables so that $\varepsilon_- = bs/t$, where $b/t \to 0$ and $b > 0$ is finite. The large parameter t then drops out of the evolution equation along (cd):

$$i\frac{d|\psi\rangle}{ds} = \begin{pmatrix} b + g/(2s) & \kappa/s \\ \kappa/s & -b + g/(2s) \end{pmatrix} |\psi\rangle, \tag{8}$$

where $|\psi\rangle = c_j(t)|j\rangle + c_{\tilde{j}}(t)|\tilde{j}\rangle$ with amplitudes c_j and $c_{\tilde{j}}$; s changes along a semicircle $s = Re^{i\phi}$ with $R \to \infty$, and ϕ decreases from π to 0. Parameter κ is a constant that depends on states of all spin directions in $|j\rangle$. In (8), we dropped all terms that decrease faster than $\sim 1/R$.

This evolution was already studied in Ref. [21], according to which we can disregard the vanishingly small off-diagonal terms κ/s in calculation of the diagonal elements of V':

$$|\langle j|V'|j\rangle| = e^{(1/2)\int_\pi^0 d\phi \, \langle j|(\hat{H}_j - \hat{H}_{j+1})|j\rangle} = e^{-\pi g/2}. \tag{9}$$

As for the off-diagonal elements of V', such an adiabatic approximation can be justified only if the initial state has the lower energy at $s \to -\infty$. Only then cannot the evolution along the complex time contour lead to growth

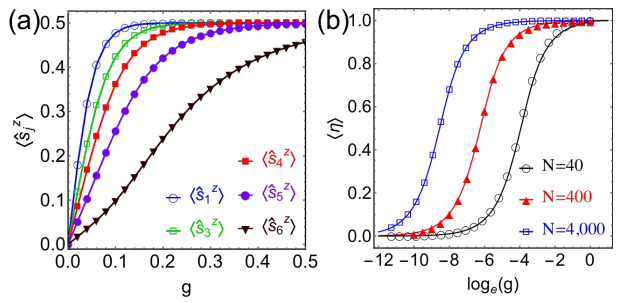

FIG. 4. **(a)** The final polarization of several spins for $N = 12$ and $S^z_{\rm tot} = 0$. Prediction of the Gibbs distribution (solid curves) is compared to numerical solution of the Schrödinger equation (point markers) [19]. Here, ε_j are the same as in Fig. 1. **(b)** Accuracy of QA at different g and N at $t \to \infty$. Points show exact predictions of Eq. (12), and solid lines are the large-N approximation (13).

of the inter-level transition amplitude [21]. For $\varepsilon_j < \varepsilon_{j+1}$ this means that

$$\langle j|V'|\tilde{j}\rangle = 0, \quad \varepsilon_j < \varepsilon_{j+1}, \tag{10}$$

independently of κ but we generally have $\langle \tilde{j}|V'|j\rangle \neq 0$. The latter element does not appear in the following calculations but we note that such a nonzero term would be relevant if the singularities were enclosed by the paths with $\mathrm{Im}(\varepsilon_-) < 0$ instead of those in Fig. 3.

Evolution along t at constant $\bar{\varepsilon}$ is the same as at ε but with exchanged spin indexes: $j \leftrightarrow j+1$. So, $\langle j|S^{\bar{\varepsilon}}|\psi_0\rangle = \langle \tilde{j}|S^{\varepsilon}|\psi_0\rangle$. The probabilities to find the microstates $|j\rangle$, $|\tilde{j}\rangle$ at fixed ε and $t \to \infty$ are then, $P_{|j\rangle} = |\langle j|S^{\varepsilon}|\psi_0\rangle|^2$ and $P_{|\tilde{j}\rangle} = |\langle j|S^{\bar{\varepsilon}}|\psi_0\rangle|^2$. Multiplying both sides of equation (5) by $\langle j|$ from the left, and using (7), (9), and (10), we find that transition probabilities from $|\psi_0\rangle$ to the two states are related:

$$P_{|\tilde{j}\rangle}/P_{|j\rangle} = e^{-2\pi g}, \quad \varepsilon_j < \varepsilon_{j+1}. \tag{11}$$

Equation (11) is valid for any index j and arbitrary values of all parameters $\varepsilon_k \notin (\varepsilon_j, \varepsilon_{j+1})$ and spin projections s^z_k in $|j\rangle$ for $k \neq j, j+1$. It has the form of the detailed balance condition that is possible to satisfy only if the probability to find any final eigenstate of $\hat{H}_A$, $|\{s^z\}\rangle \equiv |s^z_1, s^z_2, \ldots, s^z_N\rangle$, is given by the Gibbs distribution

$$P_{\{s^z\}} = \frac{1}{\mathcal{Z}} e^{-2\pi g \sum_{j=1}^N j s^z_j} \delta\left(\sum_{j=1}^N s^z_j - S^z_{\rm tot}\right), \tag{12}$$

where $1/\mathcal{Z}$ is a normalizing factor. In Fig. 4(a), we test Eq. (12) numerically and illustrate that generally spins aline along their ground state directions at $g \ll 1$, i.e., in strongly nonadiabatic regime. Independence of $P_{\{s^z\}}$ of ε_j, except the relative order of these parameters, is the property shared by many solvable time-dependent models for reasons discussed in [22]. A simpler proof of this independence is via relation (5) applied to a situation with ε and $\bar{\varepsilon}$ different only by continuous changes that keep all vector components real and nondegenerate. Pieces of evolution in Fig. 3 with $t = $ const then do not contribute to transition probabilities at all, and (5) leads to relation $|S^{\varepsilon}| = |S^{\bar{\varepsilon}}|$.

The Gibbs distribution may not describe the thermalized state of the right Hamiltonian. However, for equidistant spin splittings, $\varepsilon_j = \varepsilon j$, the distribution (12) does correspond to $\hat{H}_{\rm BCS}$ at $t \to \infty$, i.e. we find a complete thermalization in this case, as we announced in (ii), at temperature

$$T = \varepsilon/(2\pi k_B g),$$

where k_B is the Boltzmann constant.

To derive coarse-grained characteristics at $N \gg 1$, it is safe to replace the delta-function in (12) by a weaker constraint that equates only the average spin to $S^z_{\rm tot}$ (see supplementary material [19] for details of calculations, which includes Refs. [23, 24]). This leads to

$$\langle \eta \rangle \approx \frac{2}{\pi g N}(\log(1 + e^{\pi g N}) - \log 2) - 1, \tag{13}$$

which we confirm in Fig. 4(b), and from which we find that to achieve accuracy $\langle \eta \rangle$ at conditions $S^z_{\rm tot} = 0$, $N \gg 1$, $g \gg 1/N$, we should set $g = 2\log 2/[\pi N(1 - \langle \eta \rangle)]$ that is far from the adiabatic regime at $N \to \infty$, proving (i).

For example, if $g = 0.01$, i.e., calculations are 100 times faster than the adiabatically protected ones, the probability of a wrong result per spin is $(1-\langle \eta \rangle)/2 \approx 22./N$, for $N \gg 1$, and only 20-25 errors appear totally in the limit $N \to \infty$. We note that experiments with the BCS Hamiltonian in ultracold atoms deal with $N \sim 10^6$ fermions [25], in which BCS coupling can be controlled by time-dependent fields.

Our solution illustrates importance of quantum correlations that are introduced by $\hat{H}_B$: collective effects help some of the spins to settle much earlier in time (Fig. 4(a)). The remaining spins in turn feel this, which helps them to find their own ground state directions faster while satisfying the total spin conservation constraint. If, otherwise, we had set $\hat{H}_B = \sum_{i=1}^N \hat{s}^x_i$, i.e., if we were looking for the ground state of permanently uncoupled spins, we would find the final $\langle \eta \rangle$ independent of N and decaying quickly at $g < 1$, independently of the choice of ε_j.

This proves that strongly interacting QA dynamics can be studied exactly beyond the models of noninteracting fermions and their equivalents [26]. Unlike these models, simplicity of the final distribution (12) rather reflects the facts that $g(t) \sim 1/t$ is scale-free and the model (3) likely has no conservation laws, except $S^z_{\rm tot} = $ const. The latter difference leads to essentially different behavior of error probabilities in the nonadiabatic regime. Thus, the QA models that are equivalent to sets of independent two-level systems, such as the quantum Ising chain in a

transverse magnetic field [26], inevitably predict the linear scaling of the number of computational errors with growing N at other conditions fixed. In contrast, our model shows a vanishing error probability *per spin* in the limit of large N in the nonadiabatic regime at a fixed driving protocol and spin coupling distribution. This observation suggests that QA protocols with a strongly entangled initial state may provide considerable boost to accuracy of QA computations. Further experimental and numerical evidence in support of this conclusion is still needed to understand advantages of this approach.

Quantum thermalization is usually associated with semiclassical chaos that makes local operator expectations in typical eigenstates close to thermal ensemble averages [27, 28]. We showed, however, that also regular fields can steer coherent reversible evolution toward the perfect Gibbs distribution of all independent eigenstates of a Hamiltonian. Emergence of the strong detailed balance constraint, which enables this thermalization, would be impossible without the symmetry responsible for model's integrability. So, integrability is not only compatible but it is needed naturally to find the Gibbs distribution after QA. In [19], we support this conclusion by showing that the model's symmetry reflects invariance of the evolution matrix under action of the Braid Group and the associated with it quantum group $\mathrm{SU}_q(2)$ [29–31] where the deformation parameter $q \equiv e^{-\varepsilon/2k_BT}$ defines the temperature scale.

Acknowledgements. This work was carried out under the auspices of the National Nuclear Security Administration of the U.S. Department of Energy at Los Alamos National Laboratory under Contract No. DE-AC52-06NA25396 (N.A.S. and F. Li). V.Y.S. was supported by NSF Grant No. CHE-1111350 (V.Y.C.). F. Li and N.A.S. also thank the support from the LDRD program at LANL. F. Li is also supported by the Fundamental Research Funds for the Central Universities from China.

Authors declare equal contribution to this article.

[1] A. Finnila, M. Gomez, C. Sebenik, C. Stenson, and J. Doll, *Chem. Phys. Lett.* **219**, 343 (1994).
[2] G. E. Santoro, R. Martoňák, E. Tosatti, and R. Car, *Science* **295**, 2427 (2002).
[3] A. Das, and B. K. Chakrabarti, *Rev. Mod. Phys.* **80**, 1061 (2008).
[4] T. Gras, D. Raventós, B. Juliá-Daz, Christian Gogolin, and M. Lewenstein, *Nat. Comm.* **7**, 11524 (2016).
[5] S. Knysh, *Nat. Comm.* **7**, 12370 (2016).
[6] B. Gardas, J. Dziarmaga, W. H. Zurek, and M. Zwolak, *Sci. Rep.* **8**, 4539 (2018).
[7] R. Barends, *et al.*, *Nature* **534**, 222 (2016).
[8] E. Fermi, J. Pasta, S. Ulam, and M. Tsingou, Studies of the nonlinear problems, *Tech. Rep. Document* LA-1940 (Los Alamos Scientific Lab., 1955).
[9] W. Lechner, P. Hauke, and P. Zoller, *Sci. Adv.* **1**, e1500838 (2015).
[10] P. L. McMahon *et al.*, *Science* **354**, 614 (2016).
[11] S. E. Nigg, N. Lörch, and R. P. Tiwari, *Sci. Adv.* **3**, e1602273 (2017).
[12] P. W. Anderson, *Phys. Rev.* **112**, 1900 (1958).
[13] R. Matsunaga, and R. Shimano, *Phys. Rev. Lett.* **109**, 187002 (2012).
[14] R. Matsunaga, *et al.*, *Phys. Rev. Lett.* **111**, 057002 (2013).
[15] E. A. Yuzbashyan, M. Dzero, V. Gurarie, and M. S. Foster, *Phys. Rev. A* **91**, 033628 (2015).
[16] P. Kettmann, S. Hannibal, M. D. Croitoru, V. M. Axt, and T. Kuhn, *Phys. Rev.* A **96**, 033618 (2017).
[17] N. A. Sinitsyn, E. A. Yuzbashyan, V. Y. Chernyak, A. Patra, and C. Sun, *Phys. Rev. Lett.* **120**, 190402 (2018)
[18] E. A. Yuzbashyan, *Ann. Phys.* **392**, 323 (2018).
[19] In Supplementary Material, we derive characteristics of the distribution (12), discuss the Braid Group symmetry of the model, describe numerical algorithms, and compare our model to a nonintegrable one.
[20] E. A. Yuzbashyan, V. B. Kuznetsov, and B. L. Altshuler, *Phys. Rev. B* **72**, 144524 (2005).
[21] N. A. Sinitsyn, *Phys. Rev. A* **90**, 062509 (2014).
[22] V. Y. Chernyak, N. A. Sinitsyn, and Chen Sun, *J. Phys. A: Math. Theor.* **51** 245201 (2018).
[23] R. K. Pathria and P. D. Beale, *Statistical Mechanics* (Academic Press; 3rd Edition, 2011).
[24] L. D. Landau and E. M. Lifshitz, Quantum Mechanics, Third Edition: Non-Relativistic Theory (Volume 3), Butterworth-Heynemann (1981)
[25] M. Greiner, C. A. Regal, J. T. Stewart, and D. S. Jin, *Phys. Rev. Lett.* **94**, 110401 (2005).
[26] J. Dziarmaga, *Phys. Rev. Lett.* **95**, 245701 (2005).
[27] T. Kinoshita, T. Wenger, and D. S. Weiss, *Nature* **440**, 900 (2006).
[28] M. Rigol, V. Dunjko, and M. Olshanii, *Nature* **452**, 854 (2008).
[29] V. G. Drinfeld, Sov. Phys. Dokl. **283**, 1060 (1985).
[30] V. G. Drinfeld, Proc. Int. Congr. Math. Berkeley **1**, 798 (1986).
[31] V. Y. Chernyak, K. I. Grigorishin, and E. I. Ogievetsky, Phys. Lett. A **164**, 389 (1992).